PROCEEDINGS OF SPIE

Automated boundary segmentation and wound analysis for longitudinal corneal OCT images

Fei Wang, Fei Shi, Weifang Zhu, Lingjiao Pan, Haoyu Chen, et al.

SPIE.

Automated boundary segmentation and wound analysis for longitudinal corneal OCT images

Fei Wang[a], Fei Shi[a], Weifang Zhu[a], Lingjiao Pan[a], Haoyu Chen[b], Haifan Huang[b], Kangkeng Zheng[b], Xinjian Chen[a]*

[a]School of Electronic and Information Engineering, Soochow University, Suzhou, Jiangsu Province, 215006,China; [b]Joint Shantou International Eye Center of Shantou University and The Chinese University of Hong Kong, Shantou, Guangdong Province, 515041, China

ABSTRACT

Optical coherence tomography (OCT) has been widely applied in the examination and diagnosis of corneal diseases, but the information directly achieved from the OCT images by manual inspection is limited. We propose an automatic processing method to assist ophthalmologists in locating the boundaries in corneal OCT images and analyzing the recovery of corneal wounds after treatment from longitudinal OCT images. It includes the following steps: pre-processing, epithelium and endothelium boundary segmentation and correction, wound detection, corneal boundary fitting and wound analysis. The method was tested on a data set with longitudinal corneal OCT images from 20 subjects. Each subject has five images acquired after corneal operation over a period of time. The segmentation and classification accuracy of the proposed algorithm is high and can be used for analyzing wound recovery after corneal surgery.

Keywords: corneal imaging, boundary segmentation, wound detection, wound analysis, optical coherence tomography (OCT)

1. INTRODUCTION

Optical coherence tomography (OCT) is a noninvasive, non-contact imaging technique [1]. Due to the high resolution and adjustable prop depth, OCT has been used clinically for assessment of both anterior and posterior eye diseases [2]. An anterior segment OCT can clearly show the profile and structure of cornea, which allows measurement of its thickness. Especially, the OCT examination is indispensable for wounded cornea, by which the recovery process can be assessed. To relieve the ophthalmologists of the burden of manual inspection of repeated scans, we propose a method to automatically segment the corneal boundaries, and to analyze the wound recovery from longitudinal OCT images.

The cornea is a transparent film which makes the outmost layer of the eyeball. It is vulnerable to injuries which cause corneal penetration or contusion. Diagnosis of corneal symptoms is possible by measuring and evaluation of corneal thickness. Thus, segmenting the corneal boundary is crucial. Obviously, manual segmentation is time consuming and subjective, so automatic and accurate segmentation of corneal boundary is necessary.

So far, various methods have been reported to segment cornea and have obtained satisfactory results. Rabbani et al. [3] utilized the Gaussian mixed model (GMM) to segment the corneal boundaries, which includes two components modeling the background and the corneal region respectively. Larocca et al. [4] applied graph theory and dynamic programming to searching the shortest path in corneal OCT images of assigned region to find the corneal boundary. This method can also deal with corneal images with specific artifacts. Eichel et al. [5] proposed an approach using enhanced intelligent scissors, a user interactive segmentation method, to obtain the epithelium and endothelium boundary. Eichel et al. [6] used the Prewitt edge detector to extract strong boundary points. Combined with some manual segmentation results, the best-fit curve is found as the corneal boundary. However, most of these methods focus on normal cornea, and they don't perform well when corneal wounds exist.

*Send correspondence to Xinjian Chen. E-mail: xjchen@suda.edu.cn

Fig.1 shows the corneal OCT images with wounds after corneal operation. In this paper, we propose a method that automatically segments wounded corneal boundaries, detects and quantitatively analyzes the wounds, and can thus facilitate both diagnosis and prognosis evaluation. In our work, boundary segmentation and wound region detection are effectively integrated, where the position of boundaries serve as features for wound region classification.

| (a) | (b) |
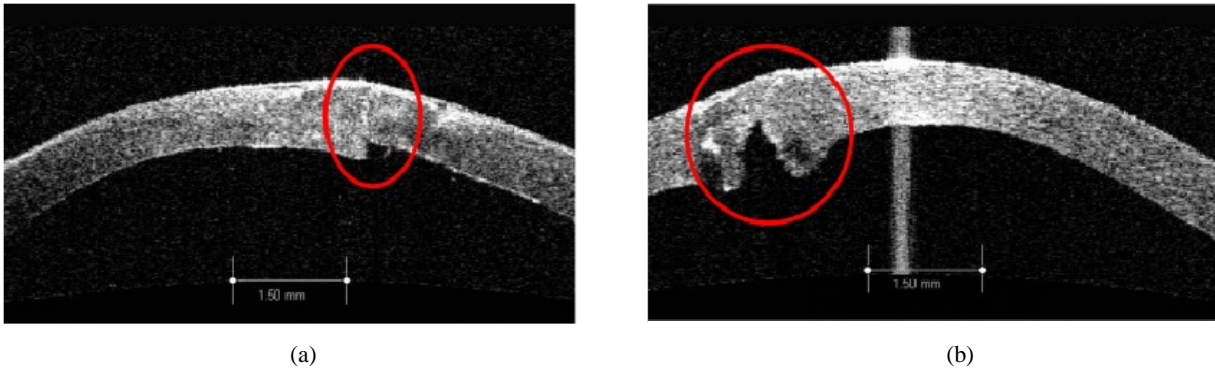
Figure 1. An anterior segment OCT image for cornea with wound after operation (obtained by ZEISS Visante OCT). (a) A corneal image with dislocation wound in the red circle. (b) A corneal image with dehiscence wound in the red circle and with central vertical artifact (discussed in Section 2.2).

2. METHODS

The proposed method includes five procedures: pre-processing, epithelium and endothelium boundary segmentation and correction, wound region detection using random forest, corneal boundary fitting and wound analysis. The details are given as follows.

2.1. Pre-processing

The corneal images acquired from the anterior segment OCT often contain other tissues such as iris and chamber angles. The images are first cropped to the same size, with these regions removed. Then, after multiplication by a coefficient 1.5 to enhance the image contrast, the Otsu thresholding is used to get a binary image. Next, several morphological operations including dilation, closing and hole filling are applied consecutively to enhance the boundaries in advance. As shown in Fig.2.

| (a) | (b) | (c) |
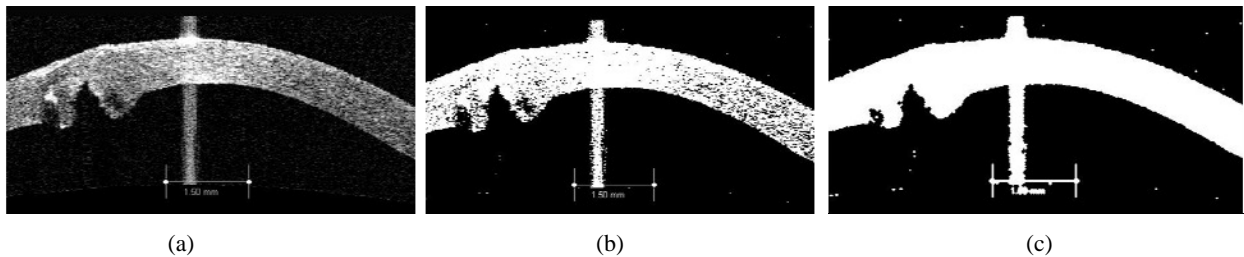
Figure 2. Preprocessing results. (a) The original image. (b) The thresholded binary image. (c) The image after morphological operation.

2.2. Epithelium and endothelium boundary segmentation and correction

The epithelium and endothelium are the upper and lower boundaries of cornea. In this step, the Canny edge detector [7] is applied on the binary image to obtain the two boundaries. The detector computes and normalizes the gradient magnitude of each pixel on the Gaussian smoothed image, then uses non-maximum suppression to thin the edges, and finally performs edge tracking with hysteresis thresholding. In this experiment, the standard deviation of Gaussian smoothing is set as 5.6, and the high and low thresholds are set as 0.96 and 0.384. The initial edge map is achieved as shown in Fig.3(a). In the edge map, the first edge point in each column is assigned as epithelium boundary point and the second edge point is assigned as endothelium boundary point.

Central vertical artifacts such as shown in Fig.1(b) will cause wrong edge detection results as shown in Fig.3(a). Therefore, a correction step is added after edge detection. Because there are only two correct boundaries in the binary edge map, the columns with more than two edge points are found as the columns corresponding to the artifacts. The boundaries in these columns are corrected by interpolation. The final boundary result is shown in Fig.3(b).

(a)   (b)
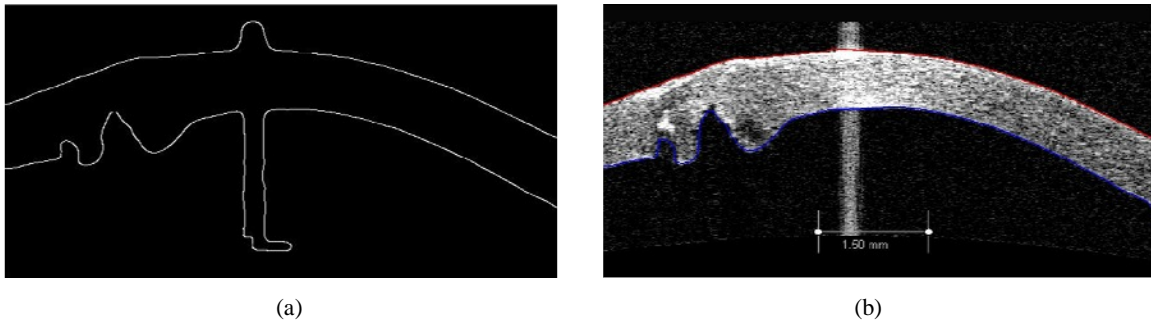
Figure 3. Detection and correction of the corneal boundaries. (a) The initial result of corneal boundary detection. (b) The boundary segmentation result after central vertical artifact correction, the red and blue curve represents the Epithelium and Endothelium boundary, respectively.

2.3.   Wound region classification using random forest

To analyze the corneal wounds, random forest classifier [8, 9] is applied to identify the wound region. Random forest classifier establishes a forest which is composed of a large number of independent decision trees, constructed in a random way. Finally the results of the classifier are produced by voting among the trees. In this experiment, we set the number of trees as 100. In the process of the classification, each column between the segmented boundaries serves as the training or testing sample. For training, the wound regions are manually labeled, supervised by an ophthalmologist. For convenience, we use the phrase corneal column to replace the meaning of each sample.

2.4.   Feature extraction

A total of 19 features are extracted from each corneal column to construct the feature vector for classification, namely the distance between boundaries, standard deviation of intensity, the distance of detected boundaries and fitting curves, four texture features generated by gray level co-occurrence matrix, and another eleven texture features generated by gray level run-length matrix.

Feature1, 2: The distance between the upper and lower boundary is a feature to capture the uneven corneal thickness. In addition, the wound scar has higher intensity than other corneal part, so the standard deviation of intensity is an outstanding feature.

Feature3, 4: We find the corneal boundaries are similar to two smooth curves except for the wound region. Based on the assumption, the detected upper and lower boundary points are fitted by two independent second-order polynomials. Feature3 is the distance between the detected upper boundary and its fitting curve. Feature4 is that for the lower boundary. For each corneal column, the greater the distance is, the more likely it belongs to corneal wound region.

Feature5, 6, 7, 8: Gray level co-occurrence matrix (GLCM) is a statistical method of examining texture that considers the spatial relationship of pixels [10, 11]. GLCM records the distribution of co-occurring pixels with a given displacement. In this method, the matrix denoted by $p(i, j)$ gives the total number of times that a pixel with gray-level i occurs vertically adjacent to a pixel with gray-level j. Computed from the matrix, four texture features are often used: contrast (CON), correlation (COR), angular second moment (ASM) and Homogeneity (HOM).

The calculation of CON is shown in (1):

$$CON = \sum_{i,j} |i - j|^2 p(i, j),$$ (1)

where i, j are the gray intensity values of the original image. CON is a measure of local variations present in the image.

The calculation of COR is shown in (2):

$$COR = \sum_{i,j} \frac{(i - \mu_i)(j - \mu_j)p(i,j)}{\sigma_i^2 \sigma_j^2},$$

(2)

where $\mu_i = \sum_{i,j} i \cdot p(i,j)$, $\mu_j = \sum_{i,j} j \cdot p(i,j)$, $\sigma_i^2 = \sum_{i,j}(i-\mu_i)^2 p(i,j)$, $\sigma_j^2 = \sum_{i,j}(j-\mu_j^2)p(i,j)$. COR is a measure of gray-level linear dependence in the image.

The calculation of ASM is shown in (3):

$$ASM = \sum_{i,j} p(i,j)^2.$$

(3)

ASM sums the squared elements in GLCM, so it is related to the homogeneity of the image.

The calculation of HOM is shown in (4):

$$HOM = \sum_{i,j} \frac{p(i,j)}{1+|i-j|}.$$

(4)

HOM measures the closeness of the distribution of elements in the GLCM to the GLCM diagonal.

Feature9-19: Gray level run-length matrix (GLRLM) is also used to extract image texture feature [12-14]. For a given image, a GLRLM $q(x, y)$ is defined as the number of runs with pixels of gray-level x and run length y. In the rough texture area, long run length has high frequency. While in the fine texture area, short run length appears more frequently. Various texture features can then be derived from this matrix. In this paper, 11 features as shown in Tab.1 are obtained from the GLRLM.

Table 1. 11 Features from the Gray Level Run Length Matrix.

Feature Name	Calculation	Feature Name	Calculation
Short Run Emphasis (SRE)	$SRE = \frac{1}{n_r}\sum_{y=1}^{N}\frac{q_r(y)}{y^2}$	Low Gray-Level Run Emphasis (LGRE)	$LGRE = \frac{1}{n_r}\sum_{x=1}^{M}\frac{q_g(x)}{x^2}$
Long Run Emphasis (LRE)	$LRE = \frac{1}{n_r}\sum_{y=1}^{N}q_r(y)\cdot y^2$	High Gray-Level Run Emphasis (HGRE)	$HGRE = \frac{1}{n_r}\sum_{x=1}^{M}q_g(x)\cdot x^2$
Gray-Level Non uniformity (GLN)	$GLN = \frac{1}{n_r}\sum_{x=1}^{M}q_g(x)^2$	Short Run Low Gray-Level Emphasis (SRLGE)	$SRLGE = \frac{1}{n_r}\sum_{x=1}^{M}\sum_{y=1}^{N}\frac{q(x,y)}{x^2 \cdot y^2}$
Run Length Non uniformity (RLN)	$RLN = \frac{1}{n_r}\sum_{y=1}^{N}q_r(y)^2$	Short Run High Gray-Level Emphasis (SRHGE)	$SRHGE = \frac{1}{n_r}\sum_{x=1}^{M}\sum_{y=1}^{N}\frac{q(x,y)\cdot x^2}{y^2}$
Run Percentage (RP)	$RP = \frac{n_r}{n_p}$	Long Run Low Gray-Level Emphasis (LRLGE)	$LRLGE = \frac{1}{n_r}\sum_{x=1}^{M}\sum_{y=1}^{N}\frac{q(x,y)\cdot y^2}{x^2}$
		Long Run High Gray-Level Emphasis (LRHGE)	$LRHGE = \frac{1}{n_r}\sum_{x=1}^{M}\sum_{y=1}^{N}q(x,y)\cdot x^2 \cdot y^2$

In the above table, M is the number of gray-level and N is the maximum run length. n_r is the total number of runs and n_p is the number of pixels in the image. $q(x, y)$ is the element of GLRLM. $q_r(x) = \sum_{y=1}^{N} q(x, y)$ is the run-length run-number vector and $q_g(x) = \sum_{x=1}^{M} q(x, y)$ is gray-level run-number vector.

2.5. Wound region detection

After the random forest classifier has been trained offline, it can be used to detect the corneal wound region. Then the continuity correction is further applied to improve the accuracy. As shown in Fig.4(a), white region marks the initially detected wound columns. Those isolated regions are removed first, then the gaps are filled and finally the white regions are connected as one continuous corneal wound region. The final result is shown in Fig.4(b).

(a)   (b)
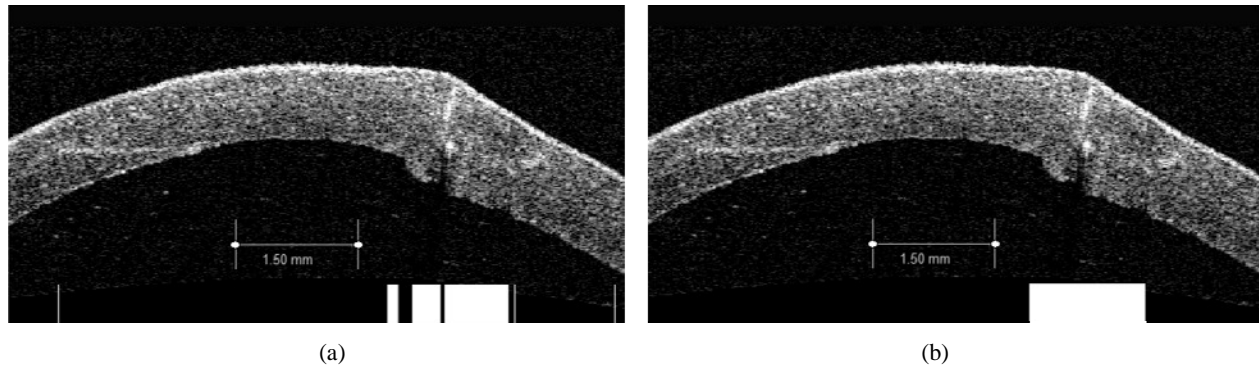
Figure 4. Wound classification and continuity correction. (a) The original classification result with random forest classifier. The white regions at the bottom indicate the detected wound region. (b) The final result of wound region classification.

2.6. Corneal boundary fitting and wound analysis

When the corneal wound position has been determined, we can assess the progress of corneal recovery after surgery. Curve fitting is performed again for the two boundaries. But different from that in Section 2.3.1, the boundary points in the detected wound regions are excluded so that the fitting curves can approximate the shape of the healed cornea. As shown in Fig.5, the red and blue curves are the segmented boundary of wounded cornea, the cyan curves are the predicted healed corneal boundaries. We calculate the mean thickness difference (MTD) between them using (5) to quantitatively analyze the corneal recovery. Obviously, MTD is bigger for the wound region.

$$MTD = \left| mean(\left| upper - lower \right|_{seg}) - mean(\left| upper - lower \right|_{fit}) \right| \tag{5}$$
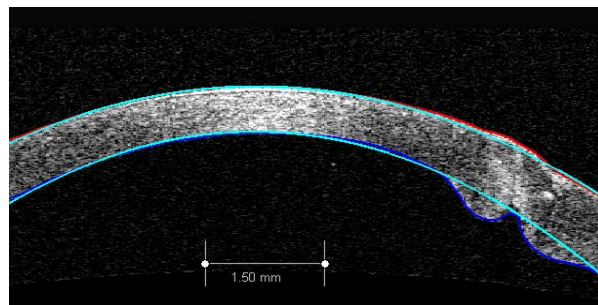
Figure 5. Curve fitting for wound recovery analysis.

3. RESULTS

In the experiment, the proposed method was tested on 20 subjects received corneal surgery. Each subject has five recovery periods. The image acquisition time points are about 0 day, 7 days, 15days, 75 days and 120 days. The OCT

image size is 318×617 pixels, with lateral resolution 0.012 mm/pixel. All the cornea data used in this experiment has only one wound region.

The mean and standard deviation of unsigned border positioning errors for epithelium and endothelium boundary are shown in Tab.2. The boundaries are segmented manually by trained observers and used as reference.

Comparing the automatic segmentation algorithm with two observers and inter-observer variability, the errors of the automatic segmentation are comparable to the inter-observer difference. The error of the endothelium segmentation is significantly bigger than epithelium due to the low edge contrast in the wound region in some images.

Table 2. Summary of mean unsigned border positioning errors for all data (in pixel).

Boundary	Algo. vs Obs1.	Algo. vs Obs2.	Obs1. vs Obs2.
Epithelium	0.75 ± 0.78	0.86 ± 0.78	0.83 ± 0.85
Endothelium	1.13 ± 1.76	1.20 ± 1.78	0.96 ± 1.15

For validation of the feasibility and effectiveness of random forest classifier, we chose the leave-one-out cross-validation method. The true positive rate (TPR), true negative rate (TNR) and the accuracy (ACC) are utilized to evaluate the classifier, computing using (6)-(8), respectively.

$$TPR = \frac{TP}{TP + FN} , \tag{6}$$

$$TNR = \frac{TN}{TN + FP} , \tag{7}$$

$$ACC = \frac{TP + TN}{TP + FP + TN + FN} , \tag{8}$$

The experimental results show that the method's average TPR is 73.9%, the average TNR is 97.4% and the average ACC is 91.7%.

Fig.6 shows the quantitative analysis of corneal wound recovery of a patient. The five cropped image slices in the upper row show the segmentation and fitting results in the wound region. The lower chart depicts the change of mean thickness difference over time. The thickness difference increases at the second time point, which is mainly due to the postoperative corneal edema caused by inflammation. In general, the decreasing trend indicates that the corneal wound is healing gradually. At the last time point, when the image shows the wound is almost completely healed, the value reaches almost zero. Therefore, it suggests that the method of curve fitting for analyzing the recovery of corneal wound is feasible and reasonable.
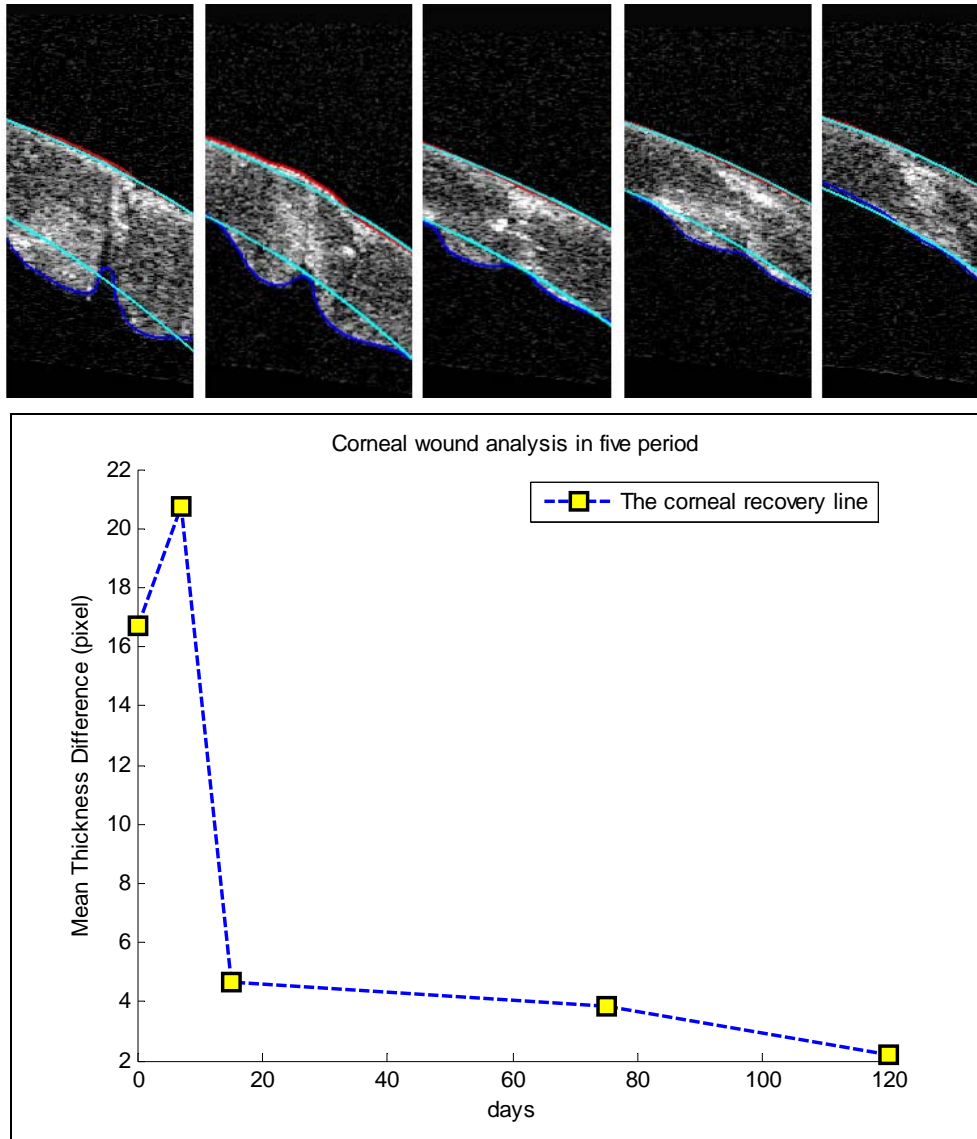
Figure 6. An example of corneal wound analysis. Square point is the mean thickness difference calculated from the segmented boundaries and fitting curves.

4. CONCLUSION AND DISCUSSION

In this paper, we propose an automatic method for segmentation and wound analysis for longitudinal corneal OCT images. Firstly, the corneal boundaries are acquired using morphological operations, Canny edge detection and correction. Then the random forest classifier is applied for identifying the wound region. Finally, the algorithm also generates the fitting curves for quantitative analysis of corneal wound. In summary, as a replacement of manual segmentation, the proposed algorithm is promising in assisting diagnosis and prognosis evaluation of patients who undergo corneal surgery. However, poor image quality can affect the performance of the proposed algorithm. With further optimization to enhance robustness, the algorithm will be made more suitable for clinical practice.

ACKNOWLEDGEMENTS

REFERENCES

[1] D. Huang, E. A. Swanson, C. P. Lin, J. S. Schuman, W. G. Stinson, W. Chang, M. R. Hee, T. J. Flotte, K. W. Gregory and C. A. Puliafito, "Optical Coherence Tomography," Science 254(5035), 1178-1181 (1991).

[2] C. Dai, C. Zhou, S. Fan, Z. Chen, X. Chai, Q. Ren and S. Jiao, "Optical coherence tomography for whole eye segment imaging," Optics Express 20(6), 6109-6115 (2012).

[3] H. Rabbani, R. Kafieh, M. K. Jahromi, S. Jorjandi, A. M. Dehnavi, F. Hajizadeh and A. Peyman, "Obtaining Thickness Maps of Corneal Layers Using the Optimal Algorithm for Intracorneal Layer Segmentation," International Journal of Biomedical Imaging 2016, 1420230 (2016).

[4] F. Larocca, S. J. Chiu, R. P. Mcnabb, A. N. Kuo, J. A. Izatt and S. Farsiu, "Robust automatic segmentation of corneal layer boundaries in SDOCT images using graph theory and dynamic programming," Biomedical Optics Express 2(6), 1524-1538 (2011).

[5] J. A. Eichel, A. Mishra, P. Fieguth, D. A. Clausi and K. Bizheva, "A Novel Algorithm for Extraction of the Layers of the Cornea," in Canadian Conference on Computer and Robot Vision, pp. 313-320 (2009).

[6] J. A. Eichel, K. Bizheva, D. A. Clausi and P. Fieguth, "Automated 3D reconstruction and segmentation from optical coherence tomography," in European Conference on Computer Vision, pp. 44-57 (2010).

[7] J. Canny, "A Computational Approach to Edge Detection," IEEE Transactions on Pattern Analysis and Machine Intelligence PAMI-8(6), 679-698 (1986).

[8] L. Breiman, "Random forests," Machine Learning 45(1), 5–32 (2001).

[9] T. K. Ho, "The random subspace method for constructing decision forests," IEEE Transactions on Pattern Analysis and Machine Intelligence 20(8), 832-844(1998).

[10] M. R. I. Hossain, I. Ahmed and M. H. Kabir, "Automatic Lung Tumor Detection Based on GLCM Features," in Asian Conference on Computer Vision, pp. 109-121 (2014).

[11] R. M. Haralick, K. S. Shanmugam and I. Dinstein, "Textural Features for Image Classification," IEEE Transactions on Systems, Man, and Cybernetics 3(6), 610-621 (1973).

[12] A. B. Tosun and C. Gunduzdemir, "Graph Run-Length Matrices for Histopathological Image Segmentation," IEEE Transactions on Medical Imaging 30(3), 721-732 (2011).

[13] X. Tang, "Texture information in run-length matrices," IEEE Transactions on Image Processing 7(11), 1602-1609 (1998).

[14] A. Padma and R. Sukanesh, "Automatic Classification and Segmentation of Brain Tumor in CT Images using Optimal Dominant Gray level Run length Texture Features," International Journal of Advanced Computer Science and Applications 2(10), (2011).